GLOBAL MULTIVIEW REGISTRATION USING NON-CONVEX ADMM

Sk Miraj Ahmed and Kunal N. Chaudhury

Department of Electrical Engineering, Indian Institute of Science

ABSTRACT

We consider the problem of aligning multiview scans obtained using a range scanner. The computational pipeline for this problem can be divided into two phases: (i) finding point-to-point *correspondences* between overlapping scans, and (ii) *registration* of the scans based on the correspondences. The focus of this work is on global registration in which the scans (modeled as point clouds) are required to be jointly registered in a common reference frame. We consider an optimization framework for global registration that is based on rank-constrained semidefinite programming. We propose to solve this semidefinite program using a non-convex variant of the ADMM (Alternating Direction Method of Multipliers) algorithm. This results in an efficient and scalable iterative method that requires just one eigendecompostion per iteration. We present simulations results on synthetic 3D models, using both clean and noisy correspondences. An interesting finding is that the algorithm is robust to wrong correspondences—it yields high-quality reconstructions even when a significant fraction of the correspondences are corrupted. Finally, by using ICP to infer the correspondences, we present some promising preliminary results for multiview reconstruction.

Index Terms— range scans, multiview registration, semidefinite programming, ADMM.

1. INTRODUCTION

The reconstruction of full 3D models from partial views has applications in engineering modeling, prosthetic design, and virtual reality. A range scanner is used for capturing partial surface scans of a 3D object from different viewpoints. The computational task is to build a full 3D representation by aligning the scans in a common reference frame via rotations and translations [1, 2]. The crucial information in this regard is the overlap between pairs of scans. In the context of image processing, this can be related to the familiar problem of image registration or stitching [3].

The computational pipeline for multiview reconstruction can be divided into two phases: (i) finding point-to-point *correspondences* between overlapping scans, and (ii) *registration* of the scans using the correspondences. In the popular ICP (Iterative Closest Point) algorithm [4, 5], the above subproblems are solved in a coupled manner. Since ICP is applied to two scans at a time, it inevitably suffers from error propagation. Moreover, pairwise matching fails to account for cycle-consistency relations arising from multiview constraints. Several variants of ICP [6, 7, 8], have been proposed to address these problems. The focus of this paper is on the registration problem and, in particular, the line of work in [9, 10, 11]. The proposal here was to decouple the correspondence and registration subproblems and solve them independently (possibly in an iterative fashion). In particular, it was demonstrated in [9, 11] that, based on the knowledge of the correspondences, the scans can be jointly registered using an optimization-based framework. Furthermore, it was argued in [11] using concrete examples that this so-called *global registration* is fundamentally superior to pairwise and sequential registration (as deployed in ICP and its variants).

On the technical front, it was demonstrated in [9] that the global registration problem can be reduced to an unconstrained optimization on the rotation manifold [12]. Later, it was observed in [11] that this particular manifold optimization can be cast as a rank-constrained semidefinite program (SDP). The SDP was relaxed into a tractable convex program by dropping the rank constraint, whose global minimum could be computed to any arbitrary accuracy using standard solvers [13]. A flip side of this approach is that the solution of the convex relaxation is not guaranteed to have the stipulated rank. In particular, to compute the desired rotations and translations, one is required to project the solution of the convex relaxation onto the original feasible set. This can result in sub-optimal solutions. To overcome this problem, we work with the original rank-constrained SDP in this paper. In particular, the proposal is to use a non-convex variant of the popular ADMM (Alternating Direction Method of Multipliers) algorithm for solving the rank-constrained SDP. This was motivated by the success of ADMM for convex programming [14, 15] and the recent work on non-convex ADMM [16, 17, 18]. The ADMM framework results in an efficient iterative method that essentially requires just one eigendecompostion per iteration. As a result, we can scale up the method to practical problems involving large number of scans. We report some empirical findings to demonstrate that the proposed algorithm is robust to wrong correspondences. Experimental results on 3D models [19] reveal that the multiview reconstructions obtained using our algorithm are at par with those obtained using classical ICP [4, 5] and a state-of-the-art method [8].

The rest of the paper is organized as follows. In Section 2, we consider a least-squares formulation of the global registration problem and reduce it to a rank-constrained SDP. An ADMM-based algorithm is then developed for solving the SDP. Simulations results on 3D models from the Stanford repository [19] are provided in Section 3. We conclude the paper in Section 4.

2. REGISTRATION OF POINT CLOUDS

The surface scan obtained from a range scanner is represented using a mesh [19]. While the edges and faces of the mesh capture important geometric information, we will just consider the 3D coordinates of the mesh vertices in this work. In other words, we treat each scan as a 3D point cloud. The point clouds are denoted as $\mathcal{P}_1, \ldots, \mathcal{P}_M$, where M is the total number of scans. Not every pair of point clouds overlap; we will use $i \sim j$ to denote the fact that $\mathcal{P}_i$ and $\mathcal{P}_j$ overlap. This information can be obtained using ICP, which also provides us the correspondence between overlapping mesh vertices. For $i \sim j$, let n_{ij} denote the number of overlapping vertices between $\mathcal{P}_i$ and $\mathcal{P}_j$.

E-mail: {skmiraj,kunal}@ee.iisc.ernet.in. This work was supported by a Startup Grant from IISc Bangalore and an EMR Grant SERB/F/6047/2016-2017 from the Department of Science and Technology, Government of India.

We denote the local coordinates of the overlapping points in $\mathcal{P}_i$ and $\mathcal{P}_j$ as

$$\{\boldsymbol{x}_{ij}^k : 1 \leq k \leq n_{ij}\} \quad \text{and} \quad \{\boldsymbol{x}_{ji}^k : 1 \leq k \leq n_{ij}\}.$$

Let $\mathbf{R}_i \in \mathbb{R}^{3\times 3}$ be the rotation matrix and $\boldsymbol{t}_i \in \mathbb{R}^3$ be the translation vector (relative to some reference frame) corresponding to $\mathcal{P}_i$. Ideally, when $i \sim j$, we have for $1 \leq k \leq n_{ij}$,

$$\mathbf{R}_i \boldsymbol{x}_{ij}^k + \boldsymbol{t}_i = \mathbf{R}_j \boldsymbol{x}_{ji}^k + \boldsymbol{t}_j. \tag{1}$$

That is, the local coordinates of the overlapping points are consistent with respect to the global reference frame. In practice, the relations in (1) only hold approximately due to various imperfections. The authors in [9] considered the following least-squares optimization:

$$\min \quad \sum_{i\sim j} \sum_{k=1}^{n_{ij}} \|\mathbf{R}_i \boldsymbol{x}_{ij}^k + \boldsymbol{t}_i - \mathbf{R}_j \boldsymbol{x}_{ji}^k - \boldsymbol{t}_j\|^2, \tag{2}$$

where the variables are $(\mathbf{R}_i, \boldsymbol{t}_i), 1 \leq i \leq M$. By introducing the matrix variables $\mathbf{R} = [\mathbf{R}_1 \cdots \mathbf{R}_M] \in \mathbb{R}^{3\times 3M}$ and $\mathbf{T} = [\boldsymbol{t}_1 \cdots \boldsymbol{t}_M] \in \mathbb{R}^{3\times M}$, we can write the objective in (2) as

$$\sum_{i\sim j} \sum_{k=1}^{n_{ij}} \|\mathbf{R}\boldsymbol{d}_{ij}^k + \mathbf{T}\boldsymbol{e}_{ij}\|^2, \tag{3}$$

where $\boldsymbol{d}_{ij}^k = (\boldsymbol{e}_i \otimes \mathbf{I})\boldsymbol{x}_{ij}^k - (\boldsymbol{e}_j \otimes \mathbf{I})\boldsymbol{x}_{ji}^k, \boldsymbol{e}_{ij} = \boldsymbol{e}_i - \boldsymbol{e}_j, \boldsymbol{e}_i \in \mathbb{R}^M$ is the all-zeros vector with one at the i-th position, $\mathbf{I}$ is the 3×3 identity matrix, and $\otimes$ denotes Kronecker product. For a fixed $\mathbf{R}$, the minimum of (3) is attained when $\mathbf{T} = -\mathbf{R}\mathbf{B}\mathbf{L}^\dagger$, where

$$\mathbf{L} = \sum_{i\sim j} n_{ij} \boldsymbol{e}_{ij} \boldsymbol{e}_{ij}^\top \quad \text{and} \quad \mathbf{B} = \sum_{i\sim j} \sum_{k=1}^{n_{ij}} \boldsymbol{d}_{ij}^k \boldsymbol{e}_{ij}^\top,$$

with $\mathbf{L}^\dagger$ being the Moore-Penrose pseudo-inverse of $\mathbf{L}$. Substituting $\mathbf{T} = -\mathbf{R}\mathbf{B}\mathbf{L}^\dagger$ in (3), we can write the objective as

$$\text{Trace}(\mathbf{C}\mathbf{R}^\top\mathbf{R}) = \sum_{1\leq i,j\leq M} \text{Trace}(\mathbf{C}_{ij}\mathbf{R}_i^\top\mathbf{R}_j),$$

where

$$\mathbf{D} = \sum_{i\sim j} \sum_{k=1}^{n_{ij}} \boldsymbol{d}_{ij}\boldsymbol{d}_{ij}^\top, \qquad \mathbf{C} = \mathbf{D} - \mathbf{B}\mathbf{L}^\dagger\mathbf{B}^\top,$$

and $\mathbf{C}_{ij} \in \mathbb{R}^{3\times 3}$ denotes the (i,j)-th block of $\mathbf{C}, 1 \leq i, j \leq M$. In other words, we can reduce (2) to the subproblem

$$\min_{\mathbf{R}_1,\ldots,\mathbf{R}_M} \quad \text{Trace}(\mathbf{C}\mathbf{R}^\top\mathbf{R}) \quad \text{s.t.} \quad \mathbf{R}_1, \ldots, \mathbf{R}_M \in \mathbb{SO}(3). \tag{4}$$

This is a so-called manifold optimization [12], where each variable $\mathbf{R}_i$ is constrained to live on the rotation manifold $\mathbb{SO}(3)$. Once the optimal rotations $\mathbf{R}_i^\star$ have been obtained by solving (4), the optimal translations are simply given by the columns of $\mathbf{T}^\star = -\mathbf{R}^\star\mathbf{B}\mathbf{L}^\dagger$. It was later observed in [11] that (4) can be formulated as a rank-constrained SDP if we work with the larger group $\mathbb{O}(3)$ of orthogonal transforms (which includes both rotations and reflections). This is based on the following equivalence.

Proposition 2.1. *Let $\mathbf{Q}_1, \ldots, \mathbf{Q}_M \in \mathbb{O}(3)$. Define the Gram matrix $\mathbf{G}$ of size $3M \times 3M$, where $\mathbf{G}_{ij} = \mathbf{Q}_i^\top\mathbf{Q}_j$ for $1 \leq i, j \leq M$. Then $\mathbf{G} \succeq \mathbf{0}, \mathbf{G}_{ii} = \mathbf{I}$, and rank$(\mathbf{G}) = 3$. Conversely, if $\mathbf{G}$ satisfies these three properties, then $\mathbf{G}_{ij} = \mathbf{R}_i^\top\mathbf{R}_j$ for some $\mathbf{R}_1, \ldots, \mathbf{R}_M \in \mathbb{O}(3)$.*

We reiterate that $\mathbf{G}_{ij}$ denotes the (i,j)-th block of $\mathbf{G}$ and not its (i,j)-th element. The notation $\mathbf{G} \succeq \mathbf{0}$ means that $\mathbf{G}$ is symmetric positive semidefinite, that is, all its eigenvalues are non-negative. The first claim in Proposition 2.1 can be easily verified. For the converse claim, we note that if $\mathbf{G} \succeq \mathbf{0}$ and rank$(\mathbf{G}) = 3$, then from the spectral theorem, we can write $\mathbf{G} = \lambda_1\boldsymbol{u}_1\boldsymbol{u}_1^\top + \lambda_2\boldsymbol{u}_2\boldsymbol{u}_2^\top + \lambda_3\boldsymbol{u}_3\boldsymbol{u}_3^\top$, where $\lambda_i > 0$ and $\boldsymbol{u}_i \in \mathbb{R}^{3M}$. Define $\mathbf{R} \in \mathbb{R}^{3\times 3M}$ to be

$$\mathbf{R} = \begin{bmatrix} \sqrt{\lambda_1}\boldsymbol{u}_1 & \sqrt{\lambda_2}\boldsymbol{u}_2 & \sqrt{\lambda_3}\boldsymbol{u}_3 \end{bmatrix}^\top, \tag{5}$$

and let $\mathbf{R} = [\mathbf{R}_1 \cdots \mathbf{R}_M]$, where $\mathbf{R}_i \in \mathbb{R}^{3\times 3}$. By construction, $\mathbf{G} = \mathbf{R}^\top\mathbf{R}$. Moreover, since $\mathbf{G}_{ii} = \mathbf{I}$, it follows that $\mathbf{R}_i^\top\mathbf{R}_i = \mathbf{I}$, namely, $\mathbf{R}_1, \ldots, \mathbf{R}_M \in \mathbb{O}(3)$. Using Proposition 2.1, we obtain the following reformulation of (4) with $\mathbb{SO}(3)$ replaced by $\mathbb{O}(3)$:

$$\min_{\mathbf{G}} \quad \text{Trace}(\mathbf{C}\mathbf{G}) \text{ s.t. } \mathbf{G} \succeq \mathbf{0}, \ \mathbf{G}_{ii} = \mathbf{I}, \text{ and } \text{rank}(\mathbf{G}) = 3. \tag{6}$$

In (6), the objective is linear and the constraints are convex, except for the non-convex rank constraint. By dropping the rank constraint, the authors in [11] obtained the following convex relaxation:

$$\min_{\mathbf{G}} \quad \text{Trace}(\mathbf{C}\mathbf{G}) \quad \text{s.t.} \quad \mathbf{G} \succeq \mathbf{0} \text{ and } \mathbf{G}_{ii} = \mathbf{I}. \tag{7}$$

The global optimum $\mathbf{G}^\star$ can be computed to any arbitrary accuracy using standard interior-point solvers [13]. The difficulty, however, is that $\mathbf{G}^\star$ is not guaranteed to be of rank 3. To compute the desired rotations and translations, this requires us to project (the possibly high-rank) $\mathbf{G}^\star$ onto the original feasible set in (6), which can produce sub-optimal results [11]. To overcome this problem, we work with the following equivalent formulation of (6):

$$\min_{\mathbf{G}} \quad \text{Trace}(\mathbf{C}\mathbf{G}) \text{ s.t. } \mathbf{G} \succeq \mathbf{0}, \ \mathbf{G}_{ii} = \mathbf{I}, \text{ and } \text{rank}(\mathbf{G}) \leq 3. \tag{8}$$

Proposition 2.2. *The optimization problems* (6) *and* (8) *are equivalent, namely, $\mathbf{G}^\star$ is an optimum solution of* (6) *if and only if $\mathbf{G}^\star$ is an optimal solution of* (8)*.*

Proof. The objectives in (6) and (8) are identical. On the other hand, since $\mathbf{G}_{ii} = \mathbf{I}$, we automatically have rank$(\mathbf{G}) \geq 3$. The feasible sets in (6) and (8) are thus identical as well. □

The algorithmic utility of formulation (8) will be evident shortly. We will empirically demonstrate in Section 3 that though we work with $\mathbb{O}(3)$ instead of $\mathbb{SO}(3)$, the $\mathbf{R}_1, \ldots, \mathbf{R}_M$ obtained from $\mathbf{G}^\star$ using (5) nevertheless yield satisfactory results. We recall that the optimal translations are given by $\mathbf{T}^\star = -\mathbf{R}^\star\mathbf{B}\mathbf{L}^\dagger$.

Following the success of ADMM for convex programming [14, 15], there have been recent work where the ADMM framework has been formally extended to non-convex problems [16, 17]. Preliminary theoretical results concerning the validity of such formal extensions have also been reported [18]. We now develop the non-convex ADMM solver for (8). As a first sep, note that we can write (8) as

$$\min_{\mathbf{G},\mathbf{H}} \quad \text{Trace}(\mathbf{C}\mathbf{G}) \quad \text{s.t.} \quad \mathbf{G} \in \Omega, \mathbf{H} \in \Theta, \text{ and } \mathbf{G} - \mathbf{H} = \mathbf{0}. \tag{9}$$

where Ω is the set of symmetric positive semidefinite matrices of size $3M \times 3M$ having rank at most 3, and Θ is the set of symmetric matrices of size $3M \times 3M$ whose 3×3 block diagonals are $\mathbf{I}$. Note that by splitting the variables, we have separated the constraints in (8) into two distinct classes. The ADMM algorithm is particularly suited for handling such split constraints. For some fixed $\rho > 0$, the augmented Lagrangian for (9) is given by

$$\mathcal{L}_\rho(\mathbf{G}, \mathbf{H}, \mathbf{\Lambda}) = \text{Trace}(\mathbf{C}\mathbf{G}) + \text{Trace}(\mathbf{\Lambda}(\mathbf{G} - \mathbf{H})) + \frac{\rho}{2}\|\mathbf{G} - \mathbf{H}\|_{\text{F}}^2,$$

where $\|\cdot\|_{\mathrm{F}}$ is the Frobenius norm, and the symmetric matrix $\mathbf{\Lambda}$ is the dual variable for the constraint $\mathbf{G}-\mathbf{H}=\mathbf{0}$ [14]. Starting with initializations $\mathbf{H}^0$ and $\mathbf{\Lambda}^0$, the ADMM solver uses the following sequence of Gauss-Seidel updates for $k \geq 0$ [14]:

$$\mathbf{G}^{k+1} = \underset{\mathbf{G}\in\Omega}{\operatorname{argmin}}\ \mathcal{L}_\rho(\mathbf{G}, \mathbf{H}^k, \mathbf{\Lambda}^k), \tag{10}$$

$$\mathbf{H}^{k+1} = \underset{\mathbf{H}\in\Theta}{\operatorname{argmin}}\ \mathcal{L}_\rho(\mathbf{G}^{k+1}, \mathbf{H}, \mathbf{\Lambda}^k), \tag{11}$$

$$\mathbf{\Lambda}^{k+1} = \mathbf{\Lambda}^k + \rho(\mathbf{G}^{k+1} - \mathbf{H}^{k+1}). \tag{12}$$

Note that we can write the objective in (10) as $(\rho/2)\|\mathbf{G} - (\mathbf{H}^k - \rho^{-1}(\mathbf{C}+\mathbf{\Lambda}^k))\|_{\mathrm{F}}^2$ plus some constant. Therefore,

$$\mathbf{G}^{k+1} = \Pi_\Omega(\mathbf{H}^k - \rho^{-1}(\mathbf{C}+\mathbf{\Lambda}^k)), \tag{13}$$

where we use $\Pi_\Omega(\mathbf{A})$ to denote the projection of $\mathbf{A}$ onto Ω, namely,

$$\Pi_\Omega(\mathbf{A}) = \underset{\mathbf{X}\in\Omega}{\operatorname{argmin}} \|\mathbf{X}-\mathbf{A}\|_{\mathrm{F}}^2. \tag{14}$$

Similarly,

$$\mathbf{H}^{k+1} = \Pi_\Theta(\mathbf{G}^{k+1} + \rho^{-1}\mathbf{\Lambda}^k). \tag{15}$$

By adapting the Eckart-Young theorem [20] for positive semidefinite matrices, we get the following result.

Theorem 2.3. *Let $\mathbf{A} = \lambda_1 \boldsymbol{u}_1\boldsymbol{u}_1^\top + \cdots + \lambda_{3M}\boldsymbol{u}_{3M}\boldsymbol{u}_{3M}^\top$ be the eigen-decomposition of a symmetric matrix $\mathbf{A}$, where $\lambda_1 \geq \cdots \geq \lambda_{3M}$ are the sorted eigenvalues, and $\boldsymbol{u}_1, \ldots, \boldsymbol{u}_{3M}$ are the corresponding eigenvectors. Then*

$$\Pi_\Omega(\mathbf{A}) = \sum_{i=1}^{3} \max(\lambda_i, 0)\boldsymbol{u}_i\boldsymbol{u}_i^\top.$$

In other words, we can compute $\Pi_\Omega(\mathbf{A})$ by performing the eigen-decomposition of $\mathbf{A}$ and retaining from its top three eigenvalues the ones that are positive; the remaining eigenvalues are set to zero. The utility of Proposition 2.2 is now evident. Namely, $\Pi_\Omega(\mathbf{A})$ is not well-defined if, instead of asking for the matrices in Ω to have rank at most 3, we insist that the rank be exactly 3. Indeed, if $\mathbf{A}$ has less than 3 positive eigenvalues, then the projection of $\mathbf{A}$ onto the set of positive semidefinite matrices of rank 3 does not exist (more precisely, the infimum in (14) is not attained). On the other hand, it is easy to see that $\Pi_\Theta(\mathbf{A})$ in (15) amounts to setting the diagonal blocks of $\mathbf{A}$ to $\mathbf{I}$, keeping the non-diagonal blocks fixed. In summary, the per-iteration cost is essentially that of computing an eigendecomposition, since (11) and (12) have negligible cost. As a result, we can scale up the algorithm to problems involving large number of scans. For the numerical experiments in Section 3, we set $\mathbf{\Lambda}^0 = \mathbf{0}$ and $\mathbf{H}^0$ as the output of the spectral relaxation of (6) [9, 11]. However, we noticed that the ADMM iterations converge even when we set $\mathbf{H}^0$ as the identity matrix. We defer the analysis of convergence (and optimality) to future work.

3. SIMULATIONS

To demonstrate the working of the proposed algorithm, we now present some simulations results using 3D models from the Stanford repository [19]. First, we report results concerning global registration, where the inter-scan correspondences are given. By extracting the scans from the 3D models (ground truth), we automatically have access to the correspondences. Moreover, this also allows us to simulate the real-world setup where some of the correspondences are inevitably wrong. For the registration problem, we compare the proposed non-convex ADMM with manifold optimization [9] and the convex SDP formulation [11]. We then work with the full pipeline for multiview reconstruction, where we are required to solve both the correspondence and registration problems. Needless to say, the reconstruction quality depends heavily on how well the correspondences are determined. This is precisely why we test the robustness of our algorithm to wrong correspondences. We visually compare the reconstruction from our algorithm with classical ICP [4] and the recent MAICP [8]. It was demonstrated in [8] that the latter provides state-of-the-art results.

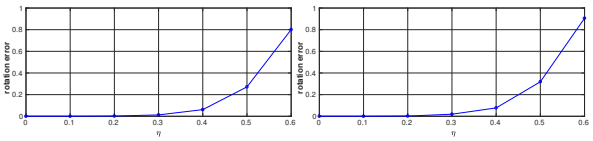

(a) Bunny. (b) Buddha.

Fig. 1. Rotation error on account of wrong correspondences for the proposed algorithm (η is the fraction of wrong correspondences). The algorithm is robust up till the 50% threshold; the reconstruction breaks down beyond that. We used 10 scans per model.

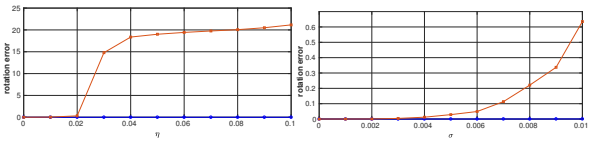

(a) Wrong correspondences (Bunny). (b) Additive noise (Bunny).

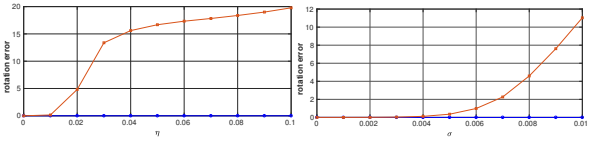

(c) Wrong correspondences (Buddha). (d) Additive noise (Buddha).

Fig. 2. Comparison of the proposed algorithm (blue line with circles) with manifold optimization (red line with squares) in terms of rotation error. We used 10 scans per model.

For the present simulations, we have used the models of Bunny and Happy Buddha [19]. The scans were recorded by rotating the model in steps of θ degrees around the z-axis. The scans are therefore $M = [360/\theta]$. We represent each scan as a point cloud extracted from the original model [9]. Each point cloud is transformed using random rotations and translations. We work with two different noise models: (i) perturbation of point-cloud coordinates, and (ii) wrong correspondences. For the noise in (i), isotropic Gaussian noise of standard deviation σ is added to the 3D coordinates of each scan point. On the other hand, for the noise in (ii), we first randomly pick a fraction $\eta \in [0,1]$ of the known correspondences, and then randomly shuffle them. To quantitatively access the reconstruction quality, we use the rotation error used in [10]. Let $\mathbf{R}_1, \ldots, \mathbf{R}_M$ denote the rotations of the initial scans relative to some reference frame, and $\mathbf{R}_1^\star, \ldots, \mathbf{R}_M^\star$ denote the rotations obtained using the proposed non-convex formulation (8). The *rotation error* (RE) is

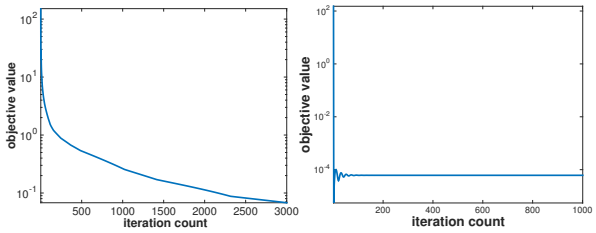

(a) Convex. (b) Non-convex.

Fig. 3. Iterations for the convex (7) and non-convex (8) formulations. In either case, the same initialization was used. The iterations in (b) converge in about 100 iterations, while the iterations in (a) converge relatively slowly. Moreover, the objective at the end of the iterations is few orders smaller for the non-convex formulation.

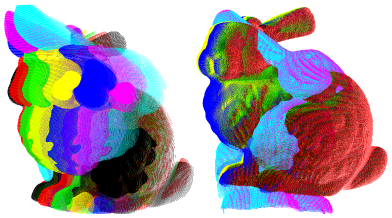

(a) Initial scans. (b) ICP [4].

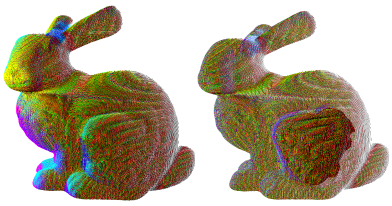

(c) Proposed. (d) MAICP [8].

Fig. 4. Reconstructions of Bunny (using 7 scans with a relative rotation of 20°). The scans are color coded for better visualization.

defined to be

$$\text{RE} = \min_{\mathbf{R}\in\mathbb{SO}(3)} \sum_{i=1}^{M} \|\mathbf{R}_i - \mathbf{R}\mathbf{R}_i^\star\|_{\text{F}}^2.$$

This measures how well the scans in the reconstruction are aligned with the initial scans. In the ideal setting, the initial scans and their reconstructions are related through a global rotation and hence the rotation error is zero. It can be shown that $\text{RE} = 6 - 2(\sigma_1 + \sigma_2 + \sigma_3)$, where σ_i's are the singular values of the cross-covariance matrix $(1/M)(\mathbf{R}_i^\star\mathbf{R}_i^\top + \cdots + \mathbf{R}_M^\star\mathbf{R}_M^\top)$ [10].

An example of the variation of RE with the number of wrong correspondences is shown in Figure 1. Surprisingly, the proposed registration can tolerate 50% outliers in the correspondences. Beyond that, the reconstruction breaks down and the error increases sharply. We compare our method with manifold optimization [9] in Figure 2, for both noise models. In the figure, η is the fraction of wrong correspondences and σ is the standard deviation of the additive noise. Notice that manifold optimization breaks down completely with just

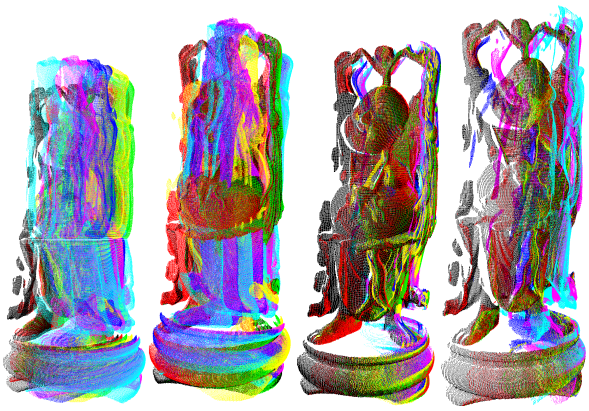

(a) Initial scans. (b) ICP [4]. (c) Proposed. (d) MAICP [8].

Fig. 5. Reconstructions of Happy Buddha from 7 scans with a relative rotation of 24°. The scans were obtained from [19].

2% wrong correspondence, whereas our method can tolerate 50% outliers. A similar trend is observed for additive noise—manifold optimization tends to break down for small perturbations. In Figure 3, we compare the convex formulation of global registration (7) and the present non-convex formulation (8). We used the same dataset for both formulations and the corresponding iterative solvers were initialized from the same point. Notice that the non-convex ADMM converges relatively quickly (this appears to be the general trend). Moreover, the optimum of the non-convex formulation is few orders smaller (recall that both formulations have the same objective). This is simply because the rank of the optimum solution of (7) turns out to be larger than d. This requires the optimum solution to be projected onto the original feasible set in (6), which results in a sub-optimal objective.

Finally, we present results for multiview reconstruction where the correspondences between scans are determined using ICP. For the experiments, we have used the 3D models of Bunny (scans were 20° apart) and Happy Buddha (scans were 24° apart). We first use ICP to align two scans. For each point in a given scan, we find its nearest neighbour in the other scan and this defines the correspondence. For the present experiments, we determine the correspondences between sequential pairs of scans (the registration is however global). The final reconstructions are compared in Figures 4 and 5. It is evident that our reconstruction is superior to ICP and and is comparable to MAICP. The reason why our algorithm works better is that the scans in both cases are quite far apart. As a result, sequential registration (which is used in ICP) fails.

4. CONCLUSION

We presented some promising results for multiview registration based on global registration. The novelty of our work was the use of non-convex ADMM for solving the SDP formulation of global registration. We gave a couple of examples where our algorithm significantly outperforms ICP and is competitive with MAICP. In particular, we demonstrated that our algorithm is robust to outliers in the correspondences. In this work, we have used sequential scan pairs for the correspondence. We expect to get better reconstructions by taking into account all pairs of overlapping scans.

5. REFERENCES

[1] R. Bergevin, M. Soucy, H. Gagnon, and D. Laurendeau, "Towards a general multi-view registration technique," *IEEE Transactions on Pattern Analysis and Machine Intelligence*, vol. 18, no. 5, pp. 540-547,1996.

[2] R. Benjemaa and F. Schmitt, "Fast global registration of 3D sampled surfaces using a multi-z-buffer technique," *Image and Vision Computing*, vol. 17, no. 2, pp. 113-123,1999.

[3] R. Szeliski, "Image alignment and stitching: A tutorial," *Foundations and Trends in Computer Graphics and Vision*, vol. 2, no. 1, pp. 1-104, 2006.

[4] P. Besl and N. McKay, "A method for registration of 3-D shapes," *IEEE Transactions on Pattern Analysis and Machine Intelligence*, vol. 14, no. 2, pp. 239-256, 1992.

[5] Y. Chen and G. Medioni, "Object modeling by registration of multiple range images," *Image and Vision Computing*, vol. 10, no. 3, pp. 145-155,1992.

[6] S. Rusinkiewicz and M. Levoy, "Efficient variants of the ICP algorithm," *Proc. IEEE International Conference on 3-D Digital Imaging and Modeling*, pp. 145-152, 2001.

[7] Q.-X. Huang and L. Guibas, "Consistent shape maps via semidefinite programming," *Computer Graphics Forum*, vol. 32, no. 5, 2013.

[8] V. M. Govindu and A. Pooja, "On averaging multiview relations for 3D scan registration," *IEEE Transactions on Image Processing*, vol. 23, no. 3, pp. 1289-1302, 2014.

[9] S. Krishnan, P. Y. Lee, J. B. Moore, and S. Venkatasubramanian, "Global registration of multiple 3D point sets via optimization-on-a-manifold," *Symposium on Geometry Processing*, pp. 187-196, 2005.

[10] T. Tzveneva, A. Singer, and S. Rusinkiewicz, "Global alignment of multiple 3-D scans using eigevector synchronization," *Technical Report*, Princeton University, 2011.

[11] K. N. Chaudhury, Y. Khoo, and A. Singer, "Global registration of multiple point clouds using semidefinite programming," *SIAM Journal on Optimization*, vol. 25, no. 1, pp. 468-501, 2015.

[12] P.-A. Absil, R. Mahony, and R. Sepulchre, *Optimization Algorithms on Matrix Manifolds*, Princeton University Press, 2009.

[13] M. Grant and S. Boyd, "CVX: Matlab software for disciplined convex programming, version 2.1," `http://cvxr.com/cvx`, 2014.

[14] S. Boyd, N. Parikh, E. Chu, B. Peleato, and J. Eckstein, "Distributed optimization and statistical learning via the alternating direction method of multipliers," *Foundations and Trends in Machine Learning*, vol. 3, no. 1, pp. 1-122, 2011.

[15] V. Cevher, S. Becker, and M. Schmidt, "Convex optimization for big data: Scalable, randomized, and parallel algorithms for big data analytics," *IEEE Signal Processing Magazine*, vol. 31, no. 5, pp. 32-43, 2014.

[16] R. Chartrand, "Nonconvex splitting for regularized low-rank + sparse decomposition," *IEEE Transactions on Signal Processing*, vol. 60, no. 11, pp. 5810-5819, 2012.

[17] O. Miksik, V. Vineet, P. Pérez, and P. S. Torr, "Distributed non-convex admm-inference in large-scale random fields," *Proc. British Machine Vision Conference*, 2014.

[18] Y. Wang, W. Yin, and J. Zeng. "Global convergence of ADMM in nonconvex nonsmooth optimization," arXiv:1511.06324, 2015.

[19] M. Levoy, "The Stanford 3D scanning repository," `https://graphics.stanford.edu/data/3Dscanrep/`, 2005.

[20] G. Eckart and G. Young, "The approximation of one matrix by another of lower rank," *Psychometrika*, vol. 1, no. 3, pp. 211-218, 1936.